Silicon (2022) 14:5157–5163
https://doi.org/10.1007/s12633-021-01307-w

ORIGINAL PAPER

The Effect of Annealing Temperature on the Structural and Optical Properties of Si/SiO_2 Composites Synthesized by Thermal Oxidation of Silicon Wafers

Kamal Kayed[1] · **Dalal Baba Kurd**[1]

Received: 24 February 2021 / Accepted: 29 July 2021 / Published online: 6 August 2021
© Springer Nature B.V. 2021

Abstract
In this article, silicon wafers were thermal treated in air at temperatures from 800 to 1200 °C. The annealed samples were investigated using X-ray diffraction, FTIR and optical reflection spectroscopy. Unique result obtained includes that possibility of employing the thermal oxidation of silicon to obtain Si/SiO_x composites with various energy gaps suitable for the manufacture of semiconductor devices. In addition, we found that the splitting of longitudinal optical and transverse optical stretching motions effect on the relative absorption coefficient. On the other hand, it has been found that, the intensity of the silicon peak in XRD spectra is proportional to the relative absorption coefficient of amorphous silicon oxide.

Keywords Silicon · Amorphous silicon oxide · FTIR · XRD · Oxidation · Van Hove singularities · Optical properties

1 Introduction

The oxidation of silicon surfaces shows promising properties that have made them the focus of many research groups [1–18], which have sought to employ various silicon oxidation techniques in the fabrication of semiconductor devices. These oxidized layers can be used as a key ingredient in creating many electronic devices such as, passivated contacts in silicon solar cells [1, 2], multi-junction quantum well solar cells [7, 8], and barrier layer in silicon-based single and passivation of the amorphous/crystalline Si (a-Si:H/c-Si) heterojunction [4–6], etc.

Thermal oxidation of silicon wafers occurs according to two different mechanisms. At high oxygen gas pressures and low temperature SiO_2 layer growth takes place (passive oxidation) according to the reaction $Si + O_2 \rightarrow SiO_2$ [17]. This oxidation method is suitable for industrial applications. In the case of low oxygen gas pressures and high temperature, SiO is desorbed in an etching process (active oxidation) according to the reaction $2Si + O_2 \rightarrow 2SiO$. In this case, the silicon surface remains free of oxide [17] with the possibility of formation of volatile SiO because of high temperature SiO_2/Si decomposition via the apparent reaction $Si + SiO_2 \rightarrow 2SiO$ when the oxygen pressure is low. On the other hand, the reoxidation reaction is also possible [17]. Silicon oxide decomposition can be used to help obtain a clean silicon surface [19], but at the same time, the electrical properties of silicon can be damaged because of this process. In fact, passive oxidation (formation of SiO_2), active oxidation (formation of SiO (gas)) and SiO_2 decomposition are considered separately, with the exception of the transition regime and the first monolayer stage of passive oxidation where these reactions are competitive. The transport of the silicon monoxide (SiO) into gas phase has been noticed only during active oxidation and oxide decomposition processes in vacuum [17]. The processes of decomposition and transition to the gas phase are important factors in determining the growth mechanism of silicon oxide layers.

In silicon oxide layers, silicon nanostructures may be present in the silicon oxide matrix. The, nucleation of Si nanoparticles is induced by a high temperature during the oxidation process. Depending on the deposition conditions and on the temperature and duration of the annealing processes, it is possible to obtain crystalline or amorphous aggregates Si-nc with different sizes and distributions embedded into a SiO*x* matrix [20]. The presence of such nanoformations in the structure of silicon oxide greatly influences its overall electrical and optical properties.

✉ Kamal Kayed
khmk2000@gmail.com

[1] Department of physics, Faculty of Science, Damascus University, Damascus, Syria

In this work, we present the results of investigating the structural and optical properties of Si/SiO_2 composites synthesized by thermal oxidation of silicon wafers, where we highlight the important effect of the thermally induced structural changes on the main features of the Kubelka-Munk curves.

2 Experimental

2.1 Sample Preparation

In order to prepare layers of silicon oxide on silicon substrates we subjected thoroughly cleaned Pure n-type Si(111) wafers (99.99%) to thermal oxidation in air using a suitable furnace. This process leads to the surface oxidation of the silicon wafers, thus obtaining oxidized surface layers (thin films). Table 1 contains the thermal treatment conditions for each sample.

2.2 Sample Characterization

The chemical composition of the samples was examined by using a FTIR spectrophotometer (JASCO- 4200) in the range 400–1300 cm^{-1}, with resolutions of 4 cm^{-1}. The crystallite structure of the films was measured by X-ray diffraction (XRD) using Philips Analytical X-Ray diffractometer employing a Cu $K\alpha_1$ ($\lambda = 1.54060$ Å) source. The optical reflection spectra were recorded with a UV–Vis spectrophotometer (Cary 5000).

3 Results and Discussion

X-ray diffraction measurements were carried out on all prepared samples. The spectra did not show any characteristic Bragg peaks for silicon oxide, indicating the amorphous structure of this oxide. Figure 1 contains a sample of the XRD spectra of all prepared samples. In all measured XRD spectra, the sharp peak located at $2\theta = 28.4^\circ$ is related to Si (111) (CSM card no. 65–1060).

Table 1 The thermal treatment conditions for each sample

Sample code	Temperature (°C)	Thermal processing time (hr)
A	–	–
B	800	4
C	900	4
D	1000	4
E	1100	4
F	1200	4

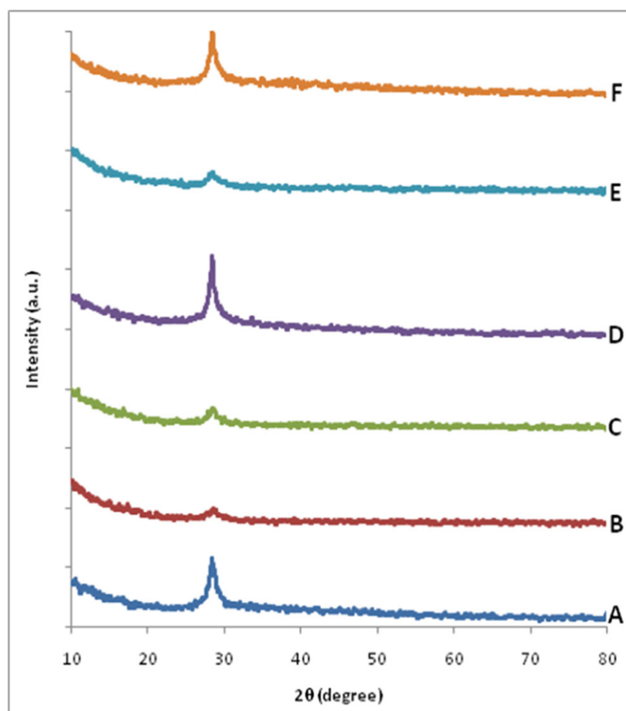

Fig. 1 The XRD spectra of all prepared samples

Figure 2 shows the infrared vibrations observed in the FTIR spectra of the annealed samples. The broad and intense band at 1000–1299 cm^{-1} and the peak at 813 cm^{-1} are attributed to asymmetric and symmetric stretching vibrations of Si-O-Si bonds [21]. The peak observed at 620 cm^{-1} is assigned to originates from the Si-Si bonds vibrations on the surface and near surface regions of porous silicon [22]. The absorption peak at 461 cm^{-1} is due to Si-O-Si rocking vibrations [21]. The weak band located at 419 cm^{-1} is due to the Si-OH bonds vibrations. The shoulder at 1190 cm^{-1} appears due to a splitting of longitudinal optical and transverse optical stretching motions [23].

We notice that, for all peaks, the intensity increases with increasing oxidation temperature, indicating that the oxidation rate increases with increasing temperature.

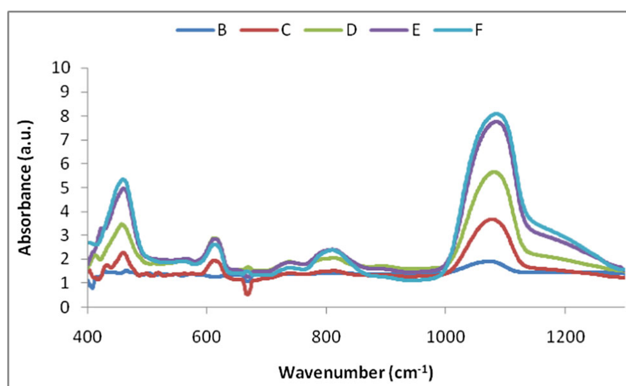

Fig. 2 Infrared absorbance spectra as a function of annealing temperature for the thermal treated samples

Figure 3 shows the reflectance spectra of the prepared samples.

We notice that, the spectra are overlapping, and for most wavelengths, the value of the reflectivity does not exceed the reflectivity in the case of the non-annealed sample (sample A). On the other hand, despite the tendency of reflectivity to decrease with increasing wavelength, the decrease associated with the appearance of two or three peaks in all spectra. In fact, these peaks do not represent overlapping fringes for the following reasons:

1. These features present in the spectrum of the non-annealed sample (sample A) that does not contain an oxide layer.
2. Based on many references, it was found that, the peaks at about 270 nm and 360 nm, corresponding to the Van Hove singularities in the density of states of crystalline silicon [24, 25]. This phenomenon is related to nanostructures close to the grain boundaries. The intensities of these peaks are proportional to the degree of crystallinity [25].
3. The peak, which appears in the spectra of the samples E and F (at 550 nm and 750 nm, respectively), is the result of the emergence of silicon nanoparticles resulting from the breaking of the long-range arrangement of silicon atoms. This distortion in the structure is caused by the splitting of longitudinal optical and transverse optical stretching motions of the bonds Si – O - Si, which was observed during the analysis of the FIR spectra (Fig. 2).

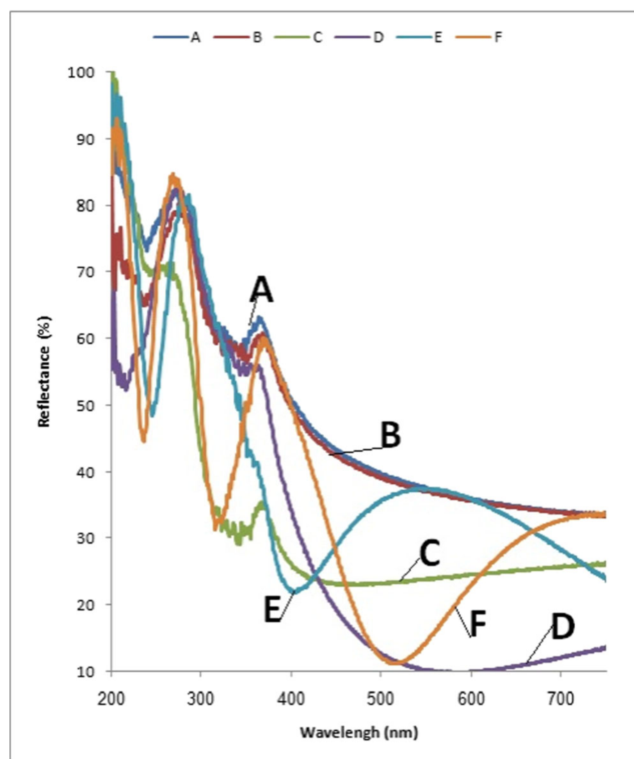

Fig. 3 The reflectance spectra of the prepared samples

The optical energy band gap (Eg) was calculated by using Tauc method, assuming direct transitions between the valence band and the conduction band. Tauc band gab can be found by plotting the variation of $(\alpha hv)^2$ against hv, where h is the energy of the incident light and α is the absorption coefficient. The extrapolation of the linear region of the curve with X-axis gives the value of optical band gap of the thin film.

In our case and because the prepared films were opaque, we calculated the absorption coefficient from the reflectance spectra using Kubelka-Munk method, which is used to describe the behavior of light travelling inside a light scattering sample [26, 27]. Figure 4 shows the method of calculating the energy band for each sample. In this figure, F(R) is a function of the reflectivity R at the wavelength λ. This function represents the absorption coefficient and given by the formula [26, 27]:

$$F(R) = \ln\left(\frac{(R_{max} - R_{min})}{(R - R_{min})}\right) \tag{1}$$

Where, R_{max} and $_{Rmin}$ are the maximum and minimum reflectivity values in the measured spectrum.

We observe that there are multiple absorption edges in each spectrum (more than one energy band gap). The calculated energy band gap values are listed in Table 2.The non-annealed sample (sample A) spectrum contains three absorption edges, one of them belonging to the silicon and the others belonging to the nanoparticles. These edges appear in the rest of the samples, despite the occurrence of oxidation processes. The absorption edge of silicon oxide appears in all spectra of the annealed samples except for the curve of sample B. However, an absorption peak of silicon oxide can be observed in sample B curve in Fig. 5, which shows the absorption coefficient as a function of the wavelength for each sample. This result indicates that the oxide molecules in sample B do not form a continuous coherent structure. On the other hand, the appearance of the silicon absorption edge in all spectra in Figs. 4 and 5 can be explained by the lack of a complete oxidation of the sample surface during the thermal treatment. These results confirm the possibility of employing the thermal oxidation of silicon to obtain Si/SiO_x composites with various energy gaps suitable for the manufacture of semiconductor devices.

Taking into account these data, we found it useful to calculate the ratio between the absorption coefficient of silicon oxide and the absorption coefficient of silicon ($\beta = F(R)_{oxide}/ F(R)_{Si}$) because it reflects the structural changes that occur due to oxidation. Figure 6 represents the relative absorption coefficient β as a function of the oxidation temperature.

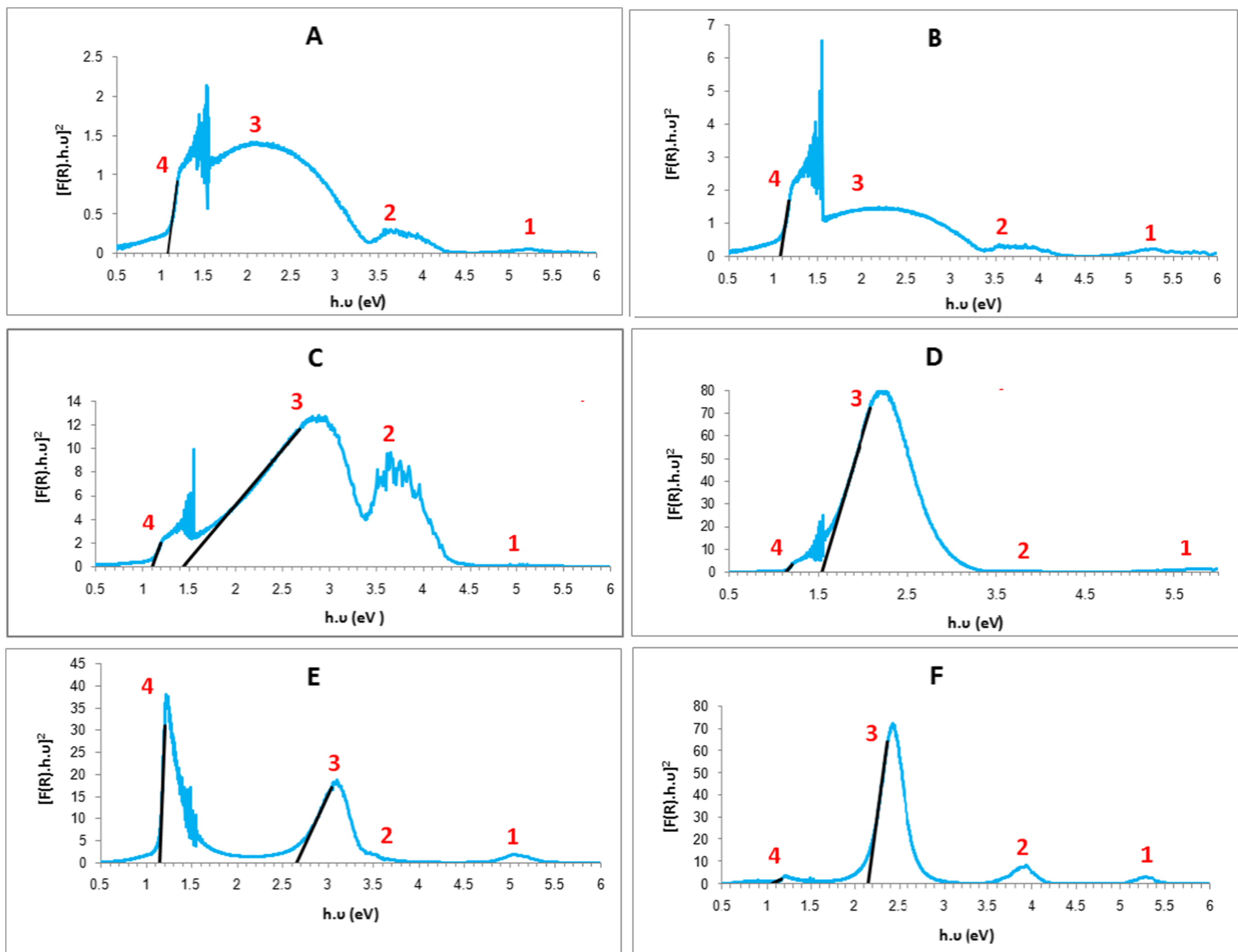

Fig. 4 Variation of (F(R).h)^2 against h for each sample. (1: NPs_1; 2: NPs_2; 3: SiO_x; 4: Si)

In this figure, β appears to increase with increasing annealing temperature within the region 800–1000 °C. The annealing at 1100 °C causes a sharp decrease in β value. Conversely, the annealing at 1200 °C leads to an increase in this parameter value. The reason for the decreasing in the β ratio of the sample E is the presence of the plasma edge that resulting from the defects in the silicon oxide structure (Fig. 3) near absorption peak of the silicon oxide (Fig. 5).

Table 2 The calculated energy band gaps for each sample

Sample code	Eg (Si)	Eg (SiO_x)
A	1.085	–
B	1.086	–
C	1.104	1.431
D	1.133	1.53
E	1.15	2.65
F	1.046	2.141

We mentioned that the silicon oxide formed due to oxidation processes is amorphous. Nevertheless, the oxide layer formed on the surface of the silicon wafer maybe affects the characteristics of the silicon peak that appear in the XRD spectra. This can be confirmed from Fig. 7, which illustrates the intensity of the silicon peak as a function of the coefficient β.

We notice that, the intensity of the silicon peak increases with increasing the relative absorption coefficient. Sample E has the lowest silicon XRD peak intensity because it contains a high concentration of crystal defects.

Figure 8 shows the optical band gap of silicon oxide as a function of annealing temperature. We notice that the band gap increases with increasing annealing temperature in the range 800–1000 °C. Once moving to the region of samples with a stressed silicon oxide structure (1100–1200 °C), the band gap begins to decrease with the increase in the annealing temperature.

Figure 9 shows the optical band gap of silicon as a function of annealing temperature. We notice that the band gap of

Fig. 5 The absorption coefficient (F(R)) as function of wavelength for each sample. (1: NPs_1; 2: NPs_2; 3: SiO_x; 4: Si)

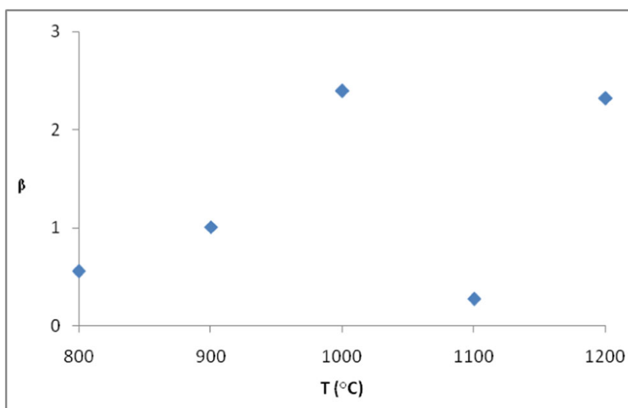

Fig. 6 The coefficient β as function of annealing temperature

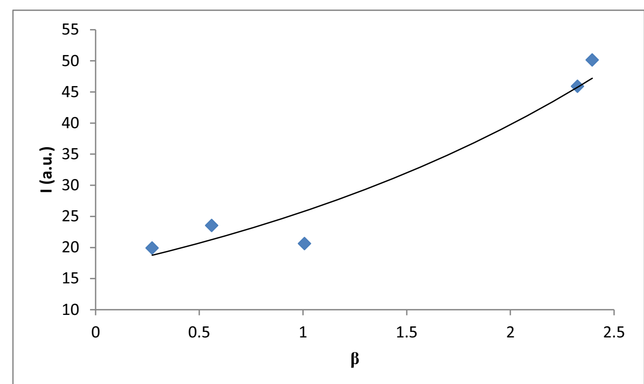

Fig. 7 The intensity of the silicon peak as a function of the coefficient β

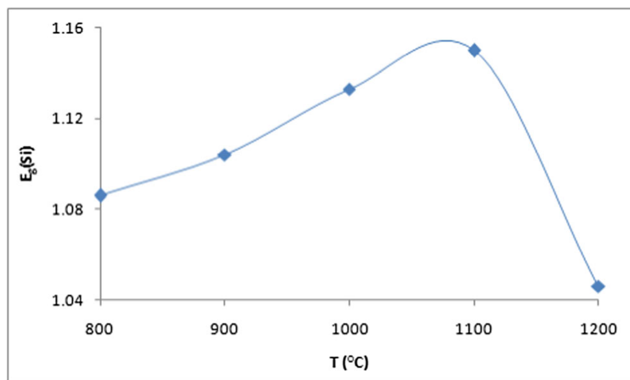

Fig. 8 The optical band gap of silicon as a function of annealing temperature

silicon also increases with increasing annealing temperature in the range 800–1100 °C. We also notice that, increasing the annealing temperature to 1200 °C decreases the energy gap value.

4 Conclusions

In this work, pure n-type Silicon (111) wafers were thermal treated at different annealing temperatures. Annealing processes were performed in the air using an oven. The effect of temperature on XRD and reflectance spectra of the prepared films was studied. The results obtained included the following:

- The thermal oxidation of silicon wafers leads to the growth of amorphous silicon oxide on the surface of silicon wafers and the rate of oxidation increases with increasing temperature.
- There are multiple absorption edges in each Kubelka-Munk curve (more than one energy band gap). These edges are located in the absorption domains of silicon, amorphous silicon oxide and silicon nanoparticles (two edges).

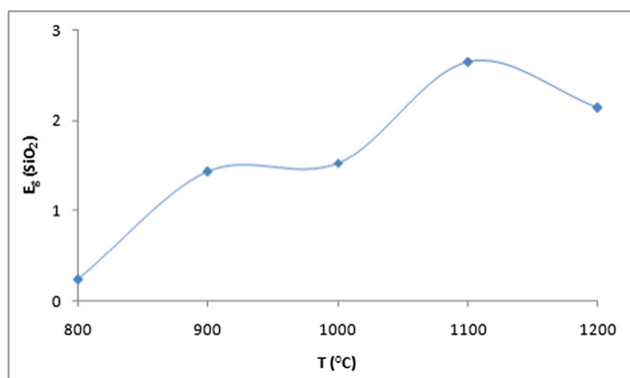

Fig. 9 The optical band gap of silicon oxide as a function of annealing temperature

- We found that the splitting of longitudinal optical and transverse optical stretching motions effect on the relative absorption coefficient.
- The intensity of the silicon peak increases with increasing the relative absorption coefficient.

Acknowledgments The authors would like to thank the University of Damascus and the Higher Institute for Applied Sciences and Technology for providing the facility to carry out this research.

Authors Contributions Dr. Kamal characterized the samples and analyzed the results of the research, and was a major contributor in writing the manuscript. Miss Dalal performed the annealing procedures and contributed to the analysis of the results and the writing of the manuscript.

Data Availability Not applicable.

Declarations

Consent with Ethical Standards This is an observational study. No ethical approval is required.

Consent to Participate Not applicable.

Consent for Publication Not applicable.

Conflict of Interests Not applicable.

References

1. Feldmann F, Bivour M, Reichel C, Steinkemper H, Hermle M, Glunz SW (2014) Tunnel oxide passivated contacts as an alternative to partial rear contacts. Sol Energy Mater Sol Cells 131:46–50
2. Moldovan A, Feldmann F, Zimmer M, Rentsch J, Benick J, Hermle M (2015) Tunnel oxide passivated carrier-selective contacts based on ultra-thin SiO_2 layers. Sol Energy Mater Sol Cells 142:123–127
3. Green MA, Godfrey RB (1976) MIS solar cell - general theory and new experimental results for silicon. APL 29:610–612
4. Bian JY, Zhang LP, Guo WW, Wang DL, Meng FY, Liu ZX (2014) Improved passivation effect at the amorphous/crystalline silicon interface due to ultrathin SiOx layers pre-formed in chemical solutions. APEX 7:065504
5. Seif JP, Descoeudres A, Filipiè M, Smole F, Topiè M, Charles Holman Z, De Wolf S, Ballif C (2014) Amorphous silicon oxide window layers for high-efficiency silicon heterojunction solar cells. J Appl Phys 115:024502
6. Ohdaira K, Oikawa T, Higashimine K, Matsumura H (2016) Suppression of the epitaxial growth of Si films in Si heterojunction solar cells by the formation of ultra-thin oxide layers. Curr Appl Phys 16:1026–1029
7. Rölver R, Berghoff B, Bätzner D, Spangenberg B, Kurz H, Schmidt M, Stegemann B (2008) Si/SiO_2 multiple quantum wells for all silicon tandem cells: conductivity and photocurrent measurements. Thin Solid Films 516:6763–6766
8. Stegemann B, Schoepke A, Schmidt M (2008) Structure and photoelectrical properties of SiO_2/Si/SiO_2 single quantum wells prepared under ultrahigh vacuum conditions. J Non-Cryst Solids 354:2100–2104

9. Grunthaner FJ, Grunthaner PJ (1986) Chemical and electronic structure of the SiO_2/Si interface. Materials Science Reports 1:65–160
10. Himpsel FJ, McFeely FR, Taleb-Ibrahimi A, Yarmoff JA, Hollinger G (1988) Microscopic structure of the SiO_2/Si interface. Phys Rev B 38:6084–6096
11. Hirose K, Nohira H, Azuma K, Hattori T (2007) Photoelectron spectroscopy studies of SiO_2/Si interfaces. Progr Surf Sci 82:3–54
12. Sieger MT, Luh DA, Miller T, Chiang TC (1996) Photoemission extended fine structure study of the SiO_{2}/Si(111) Interface. Phys Rev Lett 77:2758–2761
13. Luh DA, Miller T, Chiang TC (1997) Statistical cross-linking at the Si(111)/SiO_{2} Interface. Phys Rev Lett 79:3014–3017
14. Brower KL (1988) Kinetics of H2 passivation of Pb centers at the (111) Si-SiO_2 interface. Phys Rev B 38:9657–9666
15. Deal BE, Grove AS (1965) General relationship for the thermal oxidation of silicon. J Appl Phys 36:3770–3778
16. Hattori T (1995) Chemical structures of the SiO_2Si Interface. Crit Rev Solid State Mater Sci 20:339–382
17. Starodub D, Gusev EP, Garfunkel E, Gustafsson T (1999) Silicon oxide decomposition and desorption during the thermal oxidation of silicon. Surf Rev Lett 6:45–52
18. 1998 Fundamental Aspects of Ultrathin Dielectrics on Si-Based Devices. Garfunkel E, Gusev E, Vul A (eds). Kluwer, Dordrecht/Boston/London
19. Ishizaka A, Shiraki Y (1986) Low Temperature Surface Cleaning of Silicon and Its Application to Silicon MBE, 671. J Electrochem Soc 133:666
20. Daldosso N, Das G, Larcheri S, Mariotto G, Dalba G, Pavesi L, Irrera A, Priolo F, Iacona F, Rocca F (2007) Silicon nanocrystal formation in annealed silicon-rich silicon oxide films prepared by plasma enhanced chemical vapor deposition. J Appl Phys 101:113510
21. Chau F, Hong N, Yan C (2018) Synthesis and characterization of silicon oxide nanoparticles using an atmospheric DC plasma torch. Adv Powder Technol 2:220–229
22. Young TF, Liou JF, Chen CP, Yang YL, Chang TC (2000) Study on the Si–Si vibrational states of the near surface region of porous silicon. J Porous Mater 7:339–343
23. Lange P, Windbracke W (1989) Characterization of thermal and deposited thin oxide layers by longitudinal optical-transverse optical excitation in fourier transform IR transmission measurements. Thin Solid Films 174:159–164
24. Stern F (1963) Elementary Theory of the Optical Properties of Solids in Solid State Physics. Turnbull D, Seitz F (eds) (Academic), vol 15, pp. 299–408
25. Schmidt JA, Budini N, Rinaldi P, Arce RD, Buitrago RH (2009) Nickel-induced crystallization of amorphous silicon. J Phys Conf Ser 167:012046
26. Kubelka P, Munk F (1931) Ein beitrag zur optik der farbanstriche. Z Tech Phys 12:593–601
27. Kubelka P (1948) New contributions to the optics of intensely lightscattering materials. Part I J Opt Soc Am 38:448–457

Publisher's Note Springer Nature remains neutral with regard to jurisdictional claims in published maps and institutional affiliations.